Computers and Structures 305 (2024) 107587

Contents lists available at ScienceDirect

Computers and Structures

journal homepage: www.elsevier.com/locate/compstruc

New implicit time integration schemes for structural dynamics combining high frequency damping and high second order accuracy

Eman Alhayki *, Wulf G. Dettmer

Faculty of Science And Engineering, Swansea University, Bay Campus, Fabian Way, Swansea, SA1 8EN, Wales, United Kingdom

ARTICLE INFO

Keywords:
Implicit numerical time integration
Generalised-α method
Backward difference formula
Unconditional stability
Accuracy

ABSTRACT

The time integration schemes, GA-23 and GA-234, recently proposed by the authors for first order problems, are extended to solve second-order problems in structural dynamics. The resulting methods maintain unconditional stability and user-controlled high-frequency damping. They offer improved accuracy and exhibit less numerical damping in the low-frequency regime, outperforming the well-known generalised-α method. When the high-frequency damping is maximised the new schemes can be cast in the format of backward difference formulae, offering more accurate alternatives to the standard second order formula. The effectiveness of the new time integration schemes is validated through a number of numerical examples, including a linear elastic cantilever beam, a nonlinear spring pendulum, and wave propagation on a string.

1. Introduction

Time integration schemes are pivotal in computational engineering. Typically, these methods are divided into two categories: explicit and implicit. While explicit methods are easier to implement, they are restricted by their conditional stability [34]. In contrast, implicit methods can be designed to be unconditionally stable, providing a substantial advantage for stiff problems or simulations requiring large time steps [7].

Hilber and Hughes [15,17] identified several essential criteria for an effective numerical scheme in structural dynamics. These include unconditional stability for linear problems, efficient equation solving, second-order accuracy, controlled algorithmic dissipation, self-starting capabilities, and no overshoot behaviour. Extensive research has resulted in the development of various implicit single-step methods with these attributes, including but not limited to the Newmark-β method [31], the Wilson-θ method [37], the WBZ-α method [38], the HHT-α method [16], and the generalised-α method [8]. While these methods share common characteristics, they differ in critical aspects, such as numerical dissipation and accuracy.

Alongside these methods, multi-sub-step or composite methods have been widely adopted. These approaches require the implicit computation of multiple sets of solution variables. A prominent example is the two-sub-step Bathe method [2–4], where the trapezoidal rule is used in the first sub-step and the three-point Euler backward scheme BDF-2 in the second sub-step. This method is particularly valued for its L-stability and improved low-frequency accuracy, which significantly reduces relative period errors. However, the algorithm is computationally more demanding than single sub-step implicit methods due to the necessity of solving two sets of implicit systems within each time step. Other composite time integration schemes have been developed, as referenced in [6,26,36].

The generalised-α method has gained significant recognition for its unconditional stability, second-order accuracy in time, and user-controlled high-frequency damping through the parameter ρ_∞. Although the method was originally developed for structural dynamics [8], it has since been adapted for various fields, including computational fluid dynamics [5,12,18,20,23], fluid-structure interaction [11,13,14,19,22,35], biomechanics [24,33], general solid mechanics [1,21], and others.

For clarity of the context of the present work, it is necessary to distinguish three versions of the generalised-α method: The method was firstly introduced in the context of the second-order problem arising in structural dynamics in [8]. A related scheme, also known as the generalised-α method, was proposed in [18] for first-order problems in time and applied to computational fluid dynamics. Finally, in [21], it was shown that the application of the method from [18] to structural mechanics by means of the standard procedure based on order reduction and auxiliary sets of solution variables renders a scheme that is different from [8], but equally efficient and possesses better approximation properties.

* Corresponding author.
E-mail addresses: e.s.h.j.alhayki@swansea.ac.uk (E. Alhayki), w.g.dettmer@swansea.ac.uk (W.G. Dettmer).

https://doi.org/10.1016/j.compstruc.2024.107587
Received 22 July 2024; Accepted 11 November 2024

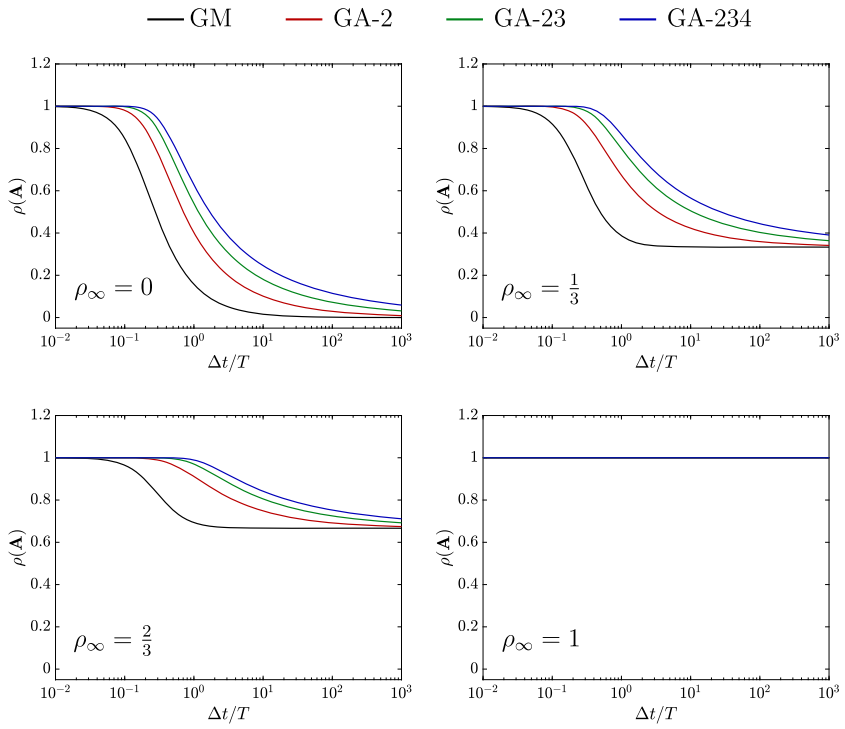

Fig. 1. Spectral radii of GM, GA-2, GA-23 and GA-234 for $\xi = 0$.

In the present article, an extended version of the generalised-α method for first-order problems, which was recently proposed by the authors in [10], is adopted to structural dynamics by following a procedure similar to [21]. The resulting schemes offer better performance than the methods presented in [8] and [21] for negligible additional computational cost. They also compete with the composite scheme presented in [3].

The remainder of this article is organised as follows: Section 2 revisits the extended family of generalised-α methods for first-order problems proposed in [10]. Section 3 details their adaptation to structural dynamics. Section 4 presents a comprehensive analysis of the schemes' properties, covering stability, accuracy, numerical dissipation, and dispersion. For maximum dissipation, the methods can be cast in the format of backward difference formula. This is shown in Section 5. Comments on the comparison between the proposed schemes and the Bathe method are provided in Section 6. The performance of the new methods is assessed in Sections 7 to 11 for various structural example systems. Conclusions are summarised in Section 12.

2. Family of generalised-α methods for first order problems

In [10], the generalised-α method for first-order problems has been reformulated and extended to include third and fourth-order accurate versions, termed GA-p, where $p = 2, 3, 4$ indicates the order of accuracy. GA-2 coincides with the generalised-α method proposed in [18] and maintains unconditional stability. The higher-order methods $p > 2$ are not unconditionally stable due to the second Dahlquist barrier [17,34]. Despite this, it has been demonstrated that linear combinations of these higher-order schemes with GA-2 yield unconditionally stable second-order methods, provided that the contribution of each higher-order method remains below a certain critical limit. This has resulted in the formulation of two new schemes denoted as GA-23 and GA-234. The former combines weighted linear combinations of GA-2 and GA-3, while the latter also includes GA-4.

The following boxes present a summary of the time integration schemes discussed in [10] for first-order initial value problems of the form

$$\dot{u}(t) - f(u(t), t) = 0, \qquad \text{with} \qquad u(0) = u_0, \tag{1}$$

where u is the solution variable, t denotes time, and $\dot{u} = \mathrm{d}u/\mathrm{d}t$. All schemes offer high frequency damping via the single user-controlled parameter ρ_∞ which represents the spectral radius of the scheme for an infinite time step size, and must be selected such that $0 \le \rho_\infty \le 1$.

Box 1 presents the generalised midpoint rule GM, which is unconditionally stable and first-order accurate. For $\rho_\infty = 0$, it recovers the first-order backward Euler method. For $\rho_\infty = 1$, it recovers the second-order trapezoidal rule, known for the minimal truncation error and absence of numerical dissipation [9].

Box 2 presents GA-2, which is equivalent to the generalised-α method proposed in [18]. By replacing the parameters α, β_0, and β_1 with α_f, α_m, and $1 - \alpha_m$ respectively, the representation of [18] is recovered.

$$\begin{aligned}
\dot{u}_{n+\alpha} &- f(u_{n+\alpha}, t_{n+\alpha}) = 0 \\
u_{n+\alpha} &= \alpha\, u_{n+1} + (1-\alpha)\, u_n \\
\dot{u}_{n+\alpha} &= \frac{u_{n+1} - u_n}{\Delta t} \\
\alpha &= \frac{1}{1+\rho_\infty}
\end{aligned}$$

Box 1. Summary of GM for first-order problems.

$$\begin{aligned}
\dot{u}_{n+\beta} &- f(u_{n+\alpha}, t_{n+\alpha}) = 0 \\
u_{n+\alpha} &= \alpha\, u_{n+1} + (1-\alpha)\, u_n \\
\dot{u}_{n+\beta} &= \beta_0\, \dot{u}_{n+1} + \beta_1\, \dot{u}_n \\
u_{n+1} &= u_n + \left(\gamma\, \dot{u}_{n+1} + (1-\gamma)\, \dot{u}_n\right) \Delta t \\
\alpha = \gamma &= \frac{1}{1+\rho_\infty}, \quad \beta_0 = \frac{3-\rho_\infty}{2(1+\rho_\infty)}, \quad \beta_1 = 1 - \beta_0
\end{aligned}$$

Box 2. Summary of GA-2 for first-order problems.

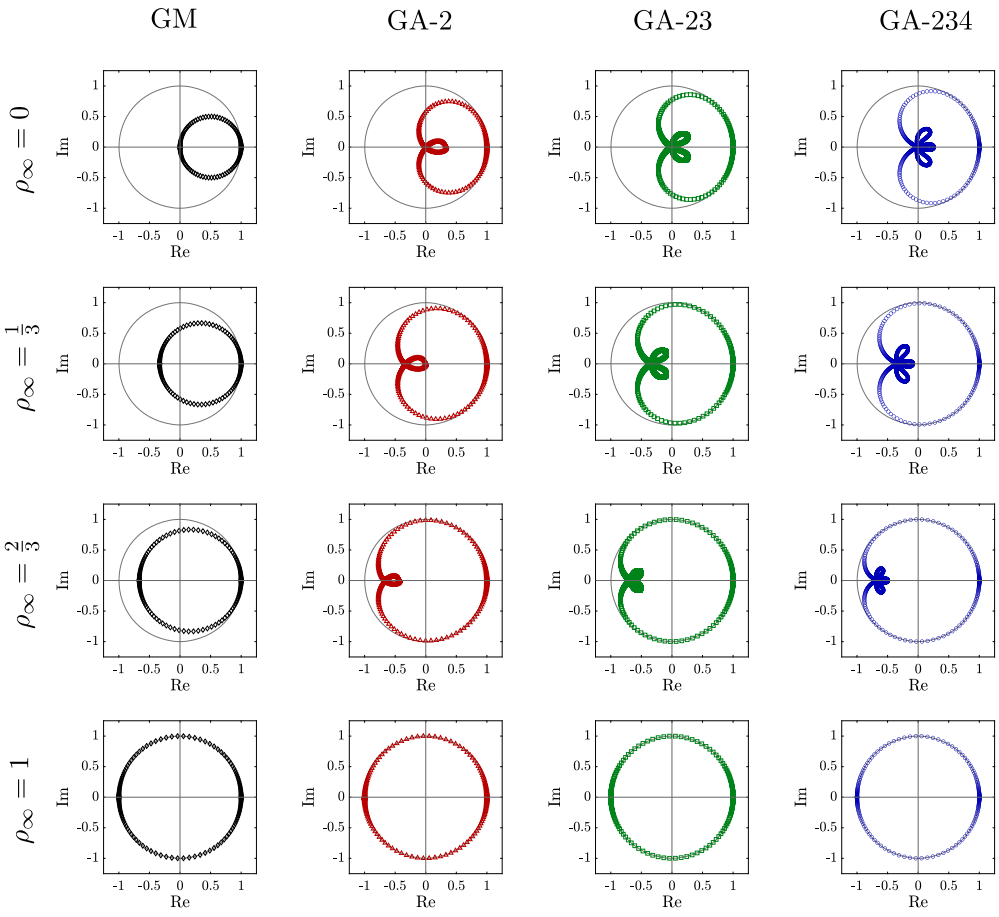

Fig. 2. Eigenvalues of GM, GA-2, GA-23 and GA-234 for $\xi = 0$, displayed in the complex plain for a range of time step sizes Δt.

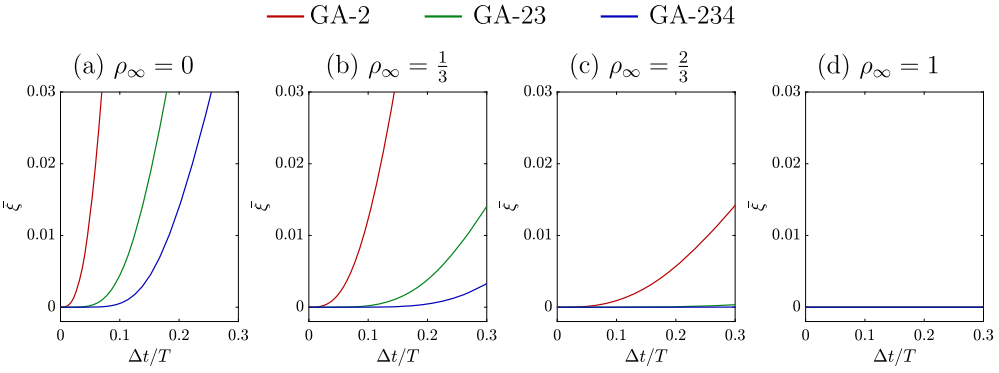

Fig. 3. Algorithmic damping ratios of GA-2, GA-23 and GA-234 for $\xi = 0$.

Boxes 3 and 4 present the new schemes GA-23 and GA-234 proposed in [10]. For $\rho_\infty < 1$, the methods outperform the generalised-α method, offering improved second-order accuracy and reduced low-frequency damping at negligible additional computational cost. For $\rho_\infty = 1$, they recover the trapezoidal rule. For $\rho_\infty = 0$, GA-23 and GA-234 recover the enhanced versions of the backward difference formula, BDF-23 and BDF-234, respectively, as shown in [10].

3. Application to structural dynamics

The methodology outlined in this section follows the procedure and notation adopted in [21] for applying first-order time integration schemes to structural dynamics. The governing equation for linear structural dynamics is expressed in matrix form as

$$\mathbf{M}\ddot{\mathbf{d}} + \mathbf{C}\dot{\mathbf{d}} + \mathbf{K}\mathbf{d} = \mathbf{F}, \tag{2}$$

where $\mathbf{M}$, $\mathbf{C}$, and $\mathbf{K}$ denote the mass, damping, and stiffness matrices respectively, and $\mathbf{F}$ is the vector of external forces. The vector $\mathbf{d}$ denotes the displacements, while $\dot{\mathbf{d}}$ and $\ddot{\mathbf{d}}$ represent the velocity and acceleration vectors respectively. The initial conditions are given as $\mathbf{d}(0) = \mathbf{d}_0$ and $\dot{\mathbf{d}}(0) = \dot{\mathbf{d}}_0$. The initial acceleration is calculated from Equation (2) as

$$\ddot{\mathbf{d}}_0 = \mathbf{M}^{-1}\left(\mathbf{F}(0) - \mathbf{C}\dot{\mathbf{d}}_0 - \mathbf{K}\mathbf{d}_0\right). \tag{3}$$

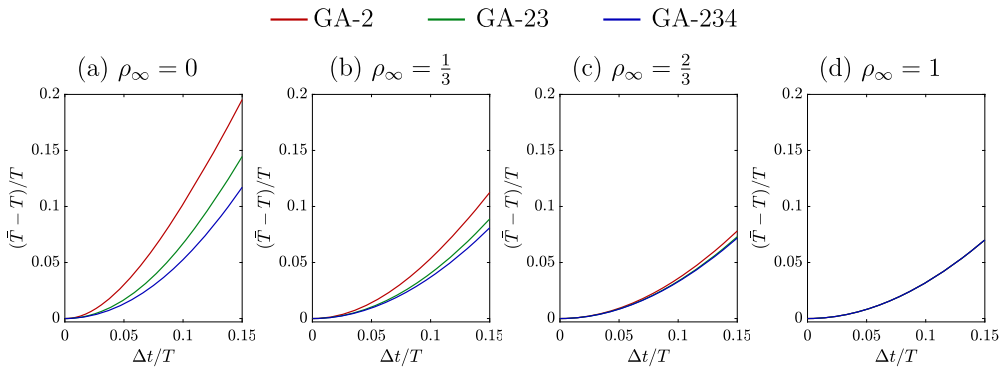

Fig. 4. Relative period error of GA-2, GA-23 and GA-234 for $\xi = 0$.

$$
\begin{aligned}
\dot{u}_{n+\beta} \;-\; f(u_{n+\alpha}, t_{n+\alpha}) \;&=\; 0 \\
u_{n+\alpha} \;&=\; \alpha\, u_{n+1} \;+\; (1-\alpha)\, u_n \\
\dot{u}_{n+\beta} \;&=\; \beta_0\, \dot{u}_{n+1} \;+\; \beta_1\, \dot{u}_n \;+\; \beta_2\, \ddot{u}_n\, \Delta t \\
u^{(i)'}_{n+1} \;&=\; u^{(i)'}_n \;+\; \left(\gamma\, u^{(i+1)'}_{n+1} \;+\; (1-\gamma)\, u^{(i+1)'}_n\right) \Delta t \quad \text{for } \; i \;=\; 0,\, 1 \\
\alpha = \gamma = \frac{1}{1+\rho_\infty},\;\; \beta_0 &= \frac{10 - 5\rho_\infty + \rho_\infty^2}{6(1+\rho_\infty)},\;\; \beta_1 = 1-\beta_0,\;\; \beta_2 = \frac{-(1-\rho_\infty)^2}{6(1+\rho_\infty)}
\end{aligned}
$$

Box 3. Summary of GA-23 for first-order problems.

$$
\begin{aligned}
\dot{u}_{n+\beta} \;-\; f(u_{n+\alpha}, t_{n+\alpha}) \;&=\; 0 \\
u_{n+\alpha} \;&=\; \alpha\, u_{n+1} + (1 \;-\; \alpha)\, u_n \\
\dot{u}_{n+\beta} \;&=\; \beta_0\, \dot{u}_{n+1} \;+\; \beta_1\, \dot{u}_n \;+\; \beta_2\, \ddot{u}_n\, \Delta t \;+\; \beta_3\, \dddot{u}_n\, \Delta t^2 \\
u^{(i)'}_{n+1} \;&=\; u^{(i)'}_n \;+\; \left(\gamma\, u^{(i+1)'}_{n+1} \;+\; (1 \;-\; \gamma)\, u^{(i+1)'}_n\right) \Delta t \qquad \text{for } i = 0, 1, 2 \\
\alpha = \gamma = \frac{1}{1+\rho_\infty},\quad \beta_0 &= \frac{35 - 21\rho_\infty + 7\rho_\infty^2 - \rho_\infty^3}{20(1+\rho_\infty)},\quad \beta_1 = 1-\beta_0, \\
\beta_2 = \frac{-(1-\rho_\infty)^2(5-\rho_\infty)}{20(1+\rho_\infty)},&\qquad \beta_3 = \frac{-(1-\rho_\infty)^3}{20(1+\rho_\infty)^2}
\end{aligned}
$$

Box 4. Summary of GA-234 for first-order problems.

$$
\begin{aligned}
\mathbf{M}\,\ddot{\mathbf{d}}_{n+\alpha} \;+\; \mathbf{C}\,\dot{\mathbf{d}}_{n+\alpha} \;+\; \mathbf{K}\,\mathbf{d}_{n+\alpha} \;&=\; \mathbf{F}_{n+\alpha} \\
\mathbf{F}_{n+\alpha} \;&=\; \alpha\,\mathbf{F}_{n+1} \;+\; (1-\alpha)\,\mathbf{F}_n \\
\mathbf{d}_{n+\alpha} \;&=\; \alpha\,\mathbf{d}_{n+1} \;+\; (1-\alpha)\,\mathbf{d}_n \\
\dot{\mathbf{d}}_{n+\alpha} \;&=\; \frac{\mathbf{d}_{n+1} \;-\; \mathbf{d}_n}{\Delta t} \\
\ddot{\mathbf{d}}_{n+\alpha} \;&=\; \frac{\dot{\mathbf{d}}_{n+1} \;-\; \dot{\mathbf{d}}_n}{\Delta t} \\
\dot{\mathbf{d}}_{n+1} \;&=\; \frac{\mathbf{d}_{n+1} \;-\; \mathbf{d}_n}{\alpha\,\Delta t} \;-\; \frac{1-\alpha}{\alpha}\,\dot{\mathbf{d}}_n
\end{aligned}
$$

Box 5. Summary of GM for structural dynamics. The coefficient α is given in Box 1.

The second-order Equation (2) is converted into a system of first-order equations by introducing the velocities $\mathbf{v}$ as auxiliary variables

$$\mathbf{v} = \dot{\mathbf{d}}, \tag{4}$$

resulting in

$$
\begin{aligned}
\mathbf{M}\,\dot{\mathbf{v}}_{n+\beta} \;+\; \mathbf{C}\,\mathbf{v}_{n+\alpha} \;+\; \mathbf{K}\,\mathbf{d}_{n+\alpha} \;&=\; \mathbf{F}_{n+\alpha} \\
\mathbf{F}_{n+\alpha} \;&=\; \alpha\,\mathbf{F}_{n+1} \;+\; (1-\alpha)\,\mathbf{F}_n \\
\mathbf{d}_{n+\alpha} \;&=\; \alpha\,\mathbf{d}_{n+1} \;+\; (1-\alpha)\,\mathbf{d}_n \\
\mathbf{v}_{n+\alpha} \;&=\; \alpha\,\mathbf{v}_{n+1} \;+\; (1-\alpha)\,\mathbf{v}_n \\
\dot{\mathbf{v}}_{n+\beta} \;&=\; \beta_0\,\dot{\mathbf{v}}_{n+1} \;+\; \beta_1\,\dot{\mathbf{v}}_n \\
\mathbf{v}_{n+1} \;&=\; \frac{1}{\alpha}\left(\beta_0\,\dot{\mathbf{d}}_{n+1} + \beta_1\,\dot{\mathbf{d}}_n - (1-\alpha)\,\mathbf{v}_n\right) \\
\dot{\mathbf{v}}_{n+1} \;&=\; \frac{\mathbf{v}_{n+1} \;-\; \mathbf{v}_n}{\Delta t\,\gamma} \;-\; \frac{1\;-\;\gamma}{\gamma}\,\dot{\mathbf{v}}_n \\
\dot{\mathbf{d}}_{n+1} \;&=\; \frac{\mathbf{d}_{n+1} \;-\; \mathbf{d}_n}{\Delta t\,\gamma} \;-\; \frac{1\;-\;\gamma}{\gamma}\,\dot{\mathbf{d}}_n
\end{aligned}
$$

Box 6. Summary of GA-2 for structural dynamics. The coefficients α, β_0, β_1 and γ are given in Box 2.

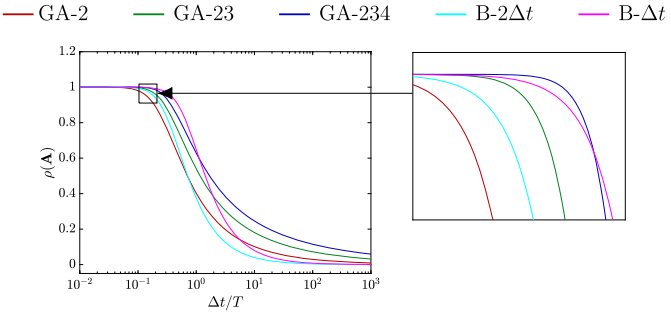

Fig. 5. Spectral radii of GA-2, GA-23, GA-234 with $\rho_\infty = 0$ and B-Δt and B-$2\Delta t$.

$$\mathbf{M}\,\dot{\mathbf{v}} + \mathbf{C}\,\mathbf{v} + \mathbf{K}\,\mathbf{d} = \mathbf{F}. \tag{5}$$

Equations (4) and (5) represent a first-order system in terms of $\mathbf{d}$ and $\mathbf{v}$. Any of the time integration schemes GM, GA-2, GA-23, and GA-234 proposed in [10], can be applied for temporal discretisation. Each method requires the implicit solution of a single set of variables.

The application of the generalised midpoint rule GM is straightforward, and the resulting equations are summarised in Box 5. Applying GA-2, GA-23, or GA-234 requires storing one, two, or three derivatives of the vectors $\mathbf{d}$ and $\mathbf{v}$, respectively. Deriving the required equations for GA-23 and GA-234 is tedious and lengthy, yet the process is straightforward and follows a procedure analogous to that used for GA-2, which is therefore described in the following. The resulting schemes for GA-2, GA-23, and GA-234 are summarised respectively in Boxes 6, 7, and 8. Note that the scheme in Box 6, is equivalent to the method described in

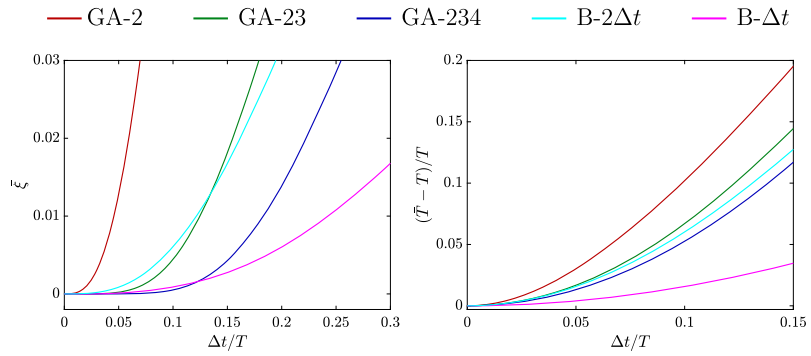

Fig. 6. Algorithmic damping ratios and relative period error of GA-2, GA-23, GA-234 with $\rho_\infty = 0$ and B-Δt and B-$2\Delta t$.

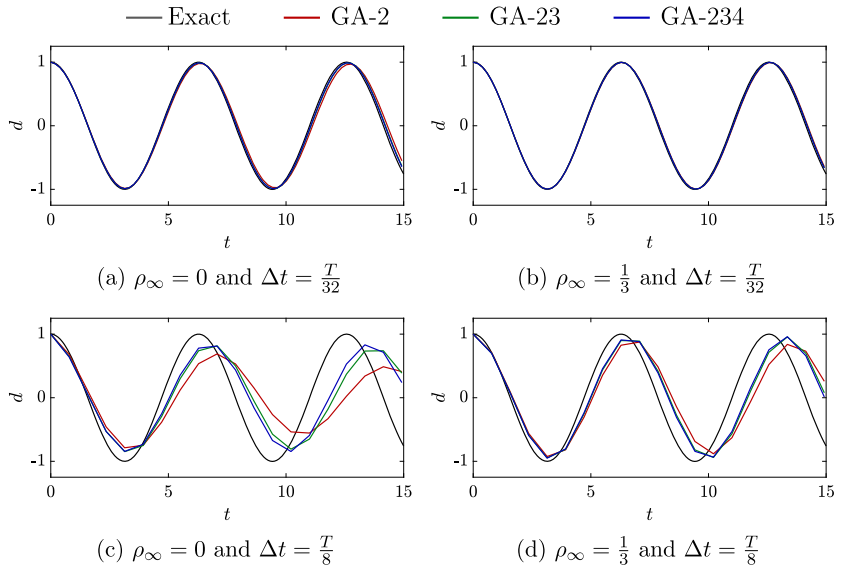

Fig. 7. Linear single degree of freedom oscillator; response obtained for $\xi = 0.0$.

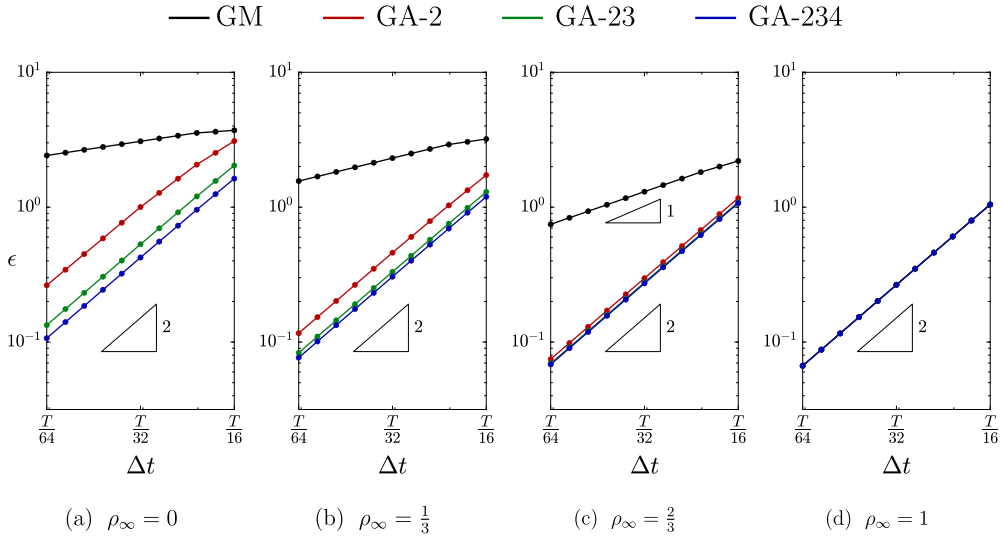

Fig. 8. Linear single degree of freedom oscillator; convergence rates.

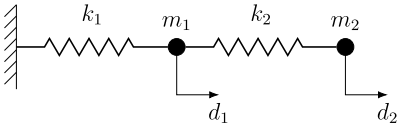

Fig. 9. Linear stiff-soft spring system, free oscillation; two-degree-of-freedom system.

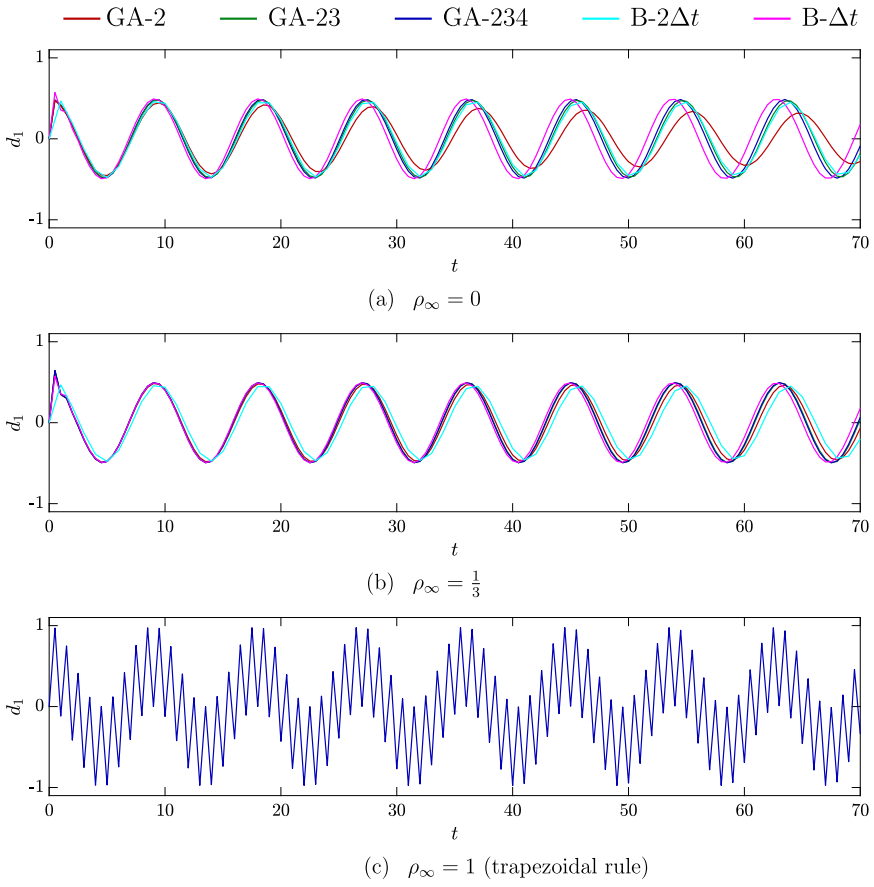

Fig. 10. Linear stiff-soft spring system, free oscillation; responses for $\Delta t = 0.5$; GA-2, GA-23, GA-234 used with different values of ρ_∞.

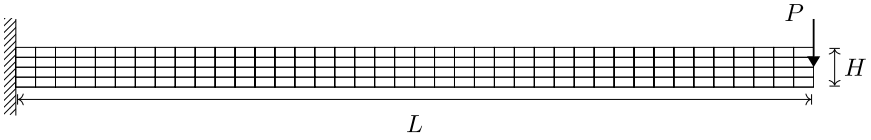

Fig. 11. Linear elastic cantilever beam; finite element mesh.

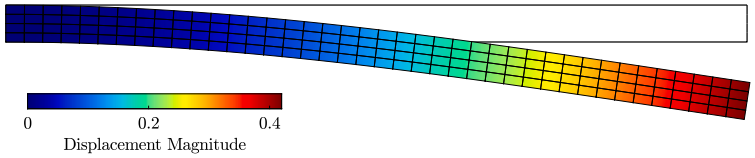

Fig. 12. Linear elastic cantilever beam; deformed and undeformed configurations.

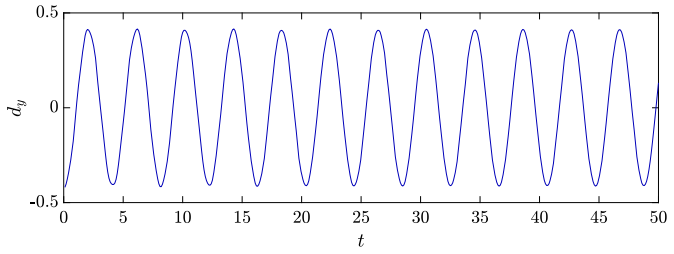

Fig. 13. Linear elastic cantilever beam; displacement over time obtained using GA-234, with $\rho_\infty = 0$ and $\Delta t = 0.1$.

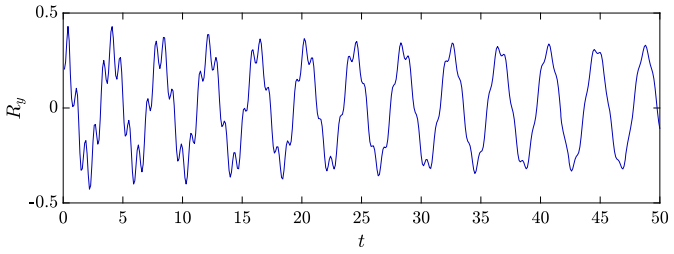

Fig. 14. Linear elastic cantilever beam; shear force over time obtained using GA-234, with $\rho_\infty = 0$ and $\Delta t = 0.1$.

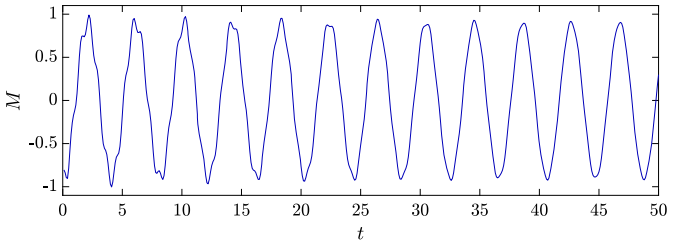

Fig. 15. Linear elastic cantilever beam; bending moment over time obtained using GA-234, with $\rho_\infty = 0$ and $\Delta t = 0.1$.

$$
\begin{aligned}
\mathbf{M}\,\dot{\mathbf{v}}_{n+\beta} + \mathbf{C}\,\mathbf{v}_{n+\alpha} + \mathbf{K}\,\mathbf{d}_{n+\alpha} &= \mathbf{F}_{n+\alpha}\\
\mathbf{F}_{n+\alpha} &= \alpha\,\mathbf{F}_{n+1} + (1-\alpha)\,\mathbf{F}_n\\
\mathbf{d}_{n+\alpha} &= \alpha\,\mathbf{d}_{n+1} + (1-\alpha)\,\mathbf{d}_n\\
\mathbf{v}_{n+\alpha} &= \alpha\,\mathbf{v}_{n+1} + (1-\alpha)\,\mathbf{v}_n\\
\dot{\mathbf{v}}_{n+\beta} &= \beta_0\,\dot{\mathbf{v}}_{n+1} + \beta_1\,\dot{\mathbf{v}}_n + \beta_2\,\ddot{\mathbf{v}}_n\,\Delta t\\
\mathbf{v}_{n+1} &= \frac{1}{\alpha}\left(\beta_0\,\dot{\mathbf{d}}_{n+1} + \beta_1\,\dot{\mathbf{d}}_n + \beta_2\,\ddot{\mathbf{d}}_n\,\Delta t - (1-\alpha)\,\mathbf{v}_n\right)\\
\mathbf{v}_{n+1}^{(i+1)'} &= \frac{\mathbf{v}_{n+1}^{(i)'} - \mathbf{v}_n^{(i)'}}{\Delta t\,\gamma} + \frac{1-\gamma}{\gamma}\,\mathbf{v}_n^{(i+1)'} \qquad \text{for} \qquad i = 0,1\\
\mathbf{d}_{n+1}^{(i+1)'} &= \frac{\mathbf{d}_{n+1}^{(i)'} - \mathbf{d}_n^{(i)'}}{\Delta t\,\gamma} + \frac{1-\gamma}{\gamma}\,\mathbf{d}_n^{(i+1)'} \qquad \text{for} \qquad i = 0,1
\end{aligned}
$$

Box 7. Summary of GA-23 for structural dynamics. The coefficients α, β_0, β_1, β_2 and γ are given in Box 3.

[21]. The schemes presented in Boxes 7 and 8 are new and represent the original contributions of this article. For nonlinear problems, the stiffness matrix $\mathbf{K}$ has to be evaluated in the configuration defined by the displacements $\mathbf{d}_{n+\alpha}$.

Applying GA-2 to Equations (4) and (5) yields the following

$$\mathbf{v}_{n+\alpha} = \dot{\mathbf{d}}_{n+\beta} \tag{6}$$

$$\mathbf{M}\,\dot{\mathbf{v}}_{n+\beta} + \mathbf{C}\,\mathbf{v}_{n+\alpha} + \mathbf{K}\,\mathbf{d}_{n+\alpha} = \mathbf{F}_{n+\alpha}, \tag{7}$$

$$
\begin{aligned}
\mathbf{M}\,\dot{\mathbf{v}}_{n+\beta} + \mathbf{C}\,\mathbf{v}_{n+\alpha} + \mathbf{K}\,\mathbf{d}_{n+\alpha} &= \mathbf{F}_{n+\alpha}\\
\mathbf{F}_{n+\alpha} &= \alpha\,\mathbf{F}_{n+1} + (1-\alpha)\,\mathbf{F}_n\\
\mathbf{d}_{n+\alpha} &= \alpha\,\mathbf{d}_{n+1} + (1-\alpha)\,\mathbf{d}_n\\
\mathbf{v}_{n+\alpha} &= \alpha\,\mathbf{v}_{n+1} + (1-\alpha)\,\mathbf{v}_n\\
\dot{\mathbf{v}}_{n+\beta} &= \beta_0\,\dot{\mathbf{v}}_{n+1} + \beta_1\,\dot{\mathbf{v}}_n + \beta_2\,\ddot{\mathbf{v}}_n\,\Delta t + \beta_3\,\dddot{\mathbf{v}}_n\,\Delta t^2\\
\mathbf{v}_{n+1} &= \frac{1}{\alpha}\left(\beta_0\,\dot{\mathbf{d}}_{n+1} + \beta_1\,\dot{\mathbf{d}}_n + \beta_2\,\ddot{\mathbf{d}}_n\,\Delta t + \beta_3\,\dddot{\mathbf{d}}_n\,\Delta t^2 - (1-\alpha)\,\mathbf{v}_n\right)\\
\mathbf{v}_{n+1}^{(i+1)'} &= \frac{\mathbf{v}_{n+1}^{(i)'} - \mathbf{v}_n^{(i)'}}{\Delta t\,\gamma} - \frac{1-\gamma}{\gamma}\,\mathbf{v}_n^{(i+1)'} \qquad \text{for} \qquad i = 0,1,2\\
\mathbf{d}_{n+1}^{(i+1)'} &= \frac{\mathbf{d}_{n+1}^{(i)'} - \mathbf{d}_n^{(i)'}}{\Delta t\,\gamma} - \frac{1-\gamma}{\gamma}\,\mathbf{d}_n^{(i+1)'} \qquad \text{for} \qquad i = 0,1,2
\end{aligned}
$$

Box 8. Summary of GA-234 for structural dynamics. The coefficients α, β_0, β_1, β_2, β_3 and γ are given in Box 4.

where

$$\mathbf{F}_{n+\alpha} = \alpha\,\mathbf{F}_{n+1} + (1-\alpha)\,\mathbf{F}_n \tag{8}$$

$$\mathbf{d}_{n+\alpha} = \alpha\,\mathbf{d}_{n+1} + (1-\alpha)\,\mathbf{d}_n \tag{9}$$

$$\dot{\mathbf{d}}_{n+\beta} = \beta_0\,\dot{\mathbf{d}}_{n+1} + \beta_1\,\dot{\mathbf{d}}_n \tag{10}$$

$$\mathbf{d}_{n+1} = \mathbf{d}_n + \Delta t\left(\gamma\,\dot{\mathbf{d}}_{n+1} + (1-\gamma)\,\dot{\mathbf{d}}_n\right) \tag{11}$$

$$\mathbf{v}_{n+\alpha} = \alpha\,\mathbf{v}_{n+1} + (1-\alpha)\,\mathbf{v}_n \tag{12}$$

$$\dot{\mathbf{v}}_{n+\beta} = \beta_0\,\dot{\mathbf{v}}_{n+1} + \beta_1\,\dot{\mathbf{v}}_n \tag{13}$$

$$\mathbf{v}_{n+1} = \mathbf{v}_n + \Delta t\left(\gamma\,\dot{\mathbf{v}}_{n+1} + (1-\gamma)\,\dot{\mathbf{v}}_n\right). \tag{14}$$

For convenience, Equations (11) and (14) are rewritten as,

$$\dot{\mathbf{d}}_{n+1} = \frac{1}{\gamma\,\Delta t}\left(\mathbf{d}_{n+1} - \mathbf{d}_n\right) - \frac{1-\gamma}{\gamma}\,\dot{\mathbf{d}}_n \tag{15}$$

$$\dot{\mathbf{v}}_{n+1} = \frac{1}{\gamma\,\Delta t}\left(\mathbf{v}_{n+1} - \mathbf{v}_n\right) - \frac{1-\gamma}{\gamma}\,\dot{\mathbf{v}}_n. \tag{16}$$

By equating $\dot{\mathbf{d}}_{n+\beta}$ and $\mathbf{v}_{n+\alpha}$ from Equations (10) and (12), $\mathbf{v}_{n+1}$ can be reformulated as

$$\mathbf{v}_{n+1} = \frac{\beta_0}{\alpha}\,\dot{\mathbf{d}}_{n+1} + \frac{\beta_1}{\alpha}\,\dot{\mathbf{d}}_n - \frac{1-\alpha}{\alpha}\,\mathbf{v}_n. \tag{17}$$

Next, by substituting Equation (15) into Equation (17), $\mathbf{v}_{n+1}$ is obtained as

$$\mathbf{v}_{n+1} = \frac{\beta_0}{\alpha\,\gamma\,\Delta t}\left(\mathbf{d}_{n+1} - \mathbf{d}_n\right) + \frac{\gamma\left(\beta_0 + \beta_1\right) - \beta_0}{\alpha\,\gamma}\,\dot{\mathbf{d}}_n - \frac{1-\alpha}{\alpha}\,\mathbf{v}_n. \tag{18}$$

Subsequently, substituting Equation (18) into Equation (16), $\dot{\mathbf{v}}_{n+1}$ becomes

$$
\begin{aligned}
\dot{\mathbf{v}}_{n+1} = {} & \frac{\beta_0}{\alpha\,\gamma^2\,\Delta t^2}\left(\mathbf{d}_{n+1} - \mathbf{d}_n\right) + \frac{\gamma\left(\beta_0 + \beta_1\right) - \beta_0}{\alpha\,\gamma^2\,\Delta t}\,\dot{\mathbf{d}}_n\\
& - \frac{1}{\alpha\,\gamma\,\Delta t}\,\mathbf{v}_n - \frac{1-\gamma}{\gamma}\,\dot{\mathbf{v}}_n.
\end{aligned} \tag{19}
$$

Finally, Equation (2) can be solved for $\mathbf{d}_{n+1}$ from

$$\hat{\mathbf{K}}\,\mathbf{d}_{n+1} = \hat{\mathbf{F}}, \tag{20}$$

where $\hat{\mathbf{K}}$ is the effective stiffness matrix

$$\hat{\mathbf{K}} = \frac{\beta_0^2}{\alpha\,\gamma^2\,\Delta t^2}\,\mathbf{M} + \frac{\beta_0}{\gamma\,\Delta t}\,\mathbf{C} + \alpha\,\mathbf{K}, \tag{21}$$

and $\hat{\mathbf{F}}$ is the effective force vector

$$\hat{\mathbf{F}} = \mathbf{F}_{n+\alpha} - \beta_1\,\mathbf{M}\,\dot{\mathbf{v}}_n - (1-\alpha)\,\mathbf{C}\,\mathbf{v}_n - (1-\alpha)\,\mathbf{K}\,\mathbf{d}_n$$

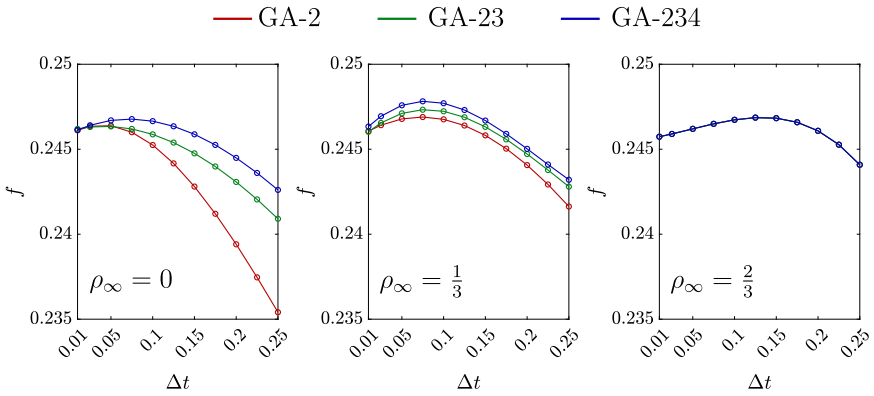

Fig. 16. Linear elastic cantilever beam; frequency convergence.

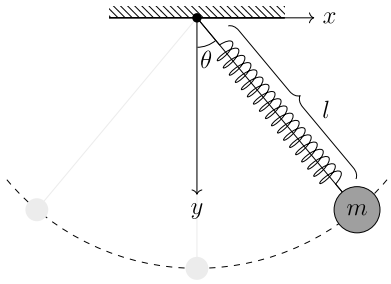

Fig. 17. Nonlinear two degree of freedom oscillator.

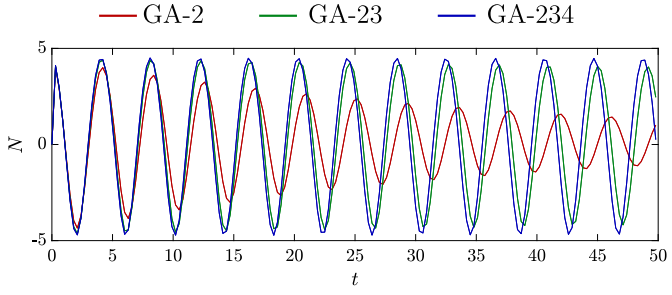

Fig. 18. Nonlinear two degree of freedom oscillator; evolution of the elastic normal force obtained using $\rho_\infty = 0$ and $\Delta t = 0.3$.

$$+\alpha\mathbf{C}\left[\frac{\beta_0}{\alpha\gamma\Delta t}\mathbf{d}_n - \frac{\gamma(\beta_0+\beta_1)-\beta_0}{\alpha\gamma}\dot{\mathbf{d}}_n + \frac{1-\alpha}{\alpha}\mathbf{v}_n\right]$$
$$+\beta_0\mathbf{M}\left[\frac{\beta_0}{\alpha\gamma^2\Delta t^2}\mathbf{d}_n - \frac{\gamma(\beta_0+\beta_1)-\beta_0}{\alpha\gamma^2\Delta t}\dot{\mathbf{d}}_n + \frac{1}{\alpha\gamma\Delta t}\mathbf{v}_n + \frac{1-\gamma}{\gamma}\dot{\mathbf{v}}_n\right]. \tag{22}$$

Once $\mathbf{d}_{n+1}$ is obtained, $\dot{\mathbf{d}}_{n+1}$, $\mathbf{v}_{n+1}$, and $\dot{\mathbf{v}}_{n+1}$ can be computed using Equations (15), (18), and (19), respectively.

4. Analysis of methods GA-23 and GA-234

This section investigates the numerical properties of the new schemes GA-23 and GA-234. The coupled equations of motion are applied to a single-degree-of-freedom system. The governing equation of an unforced system is given by

$$\ddot{d} + 2\xi\omega\dot{d} + \omega^2 d = 0, \tag{23}$$

where ω is the natural frequency, ξ is the damping ratio, and the oscillation period is defined as $T = \frac{2\pi}{\omega}$. The solutions at t_{n+1} can be expressed as

$$\mathbf{X_{n+1}} = \mathbf{A}\,\mathbf{X_n}, \tag{24}$$

where

$$\text{GA-2:}\quad \mathbf{X_n} = \left\{ d_n, v_n\Delta t, \dot{d}_n\Delta t, \dot{v}_n\Delta t^2 \right\}^T$$
$$\text{GA-23:}\quad \mathbf{X_n} = \left\{ d_n, v_n\Delta t, \dot{d}_n\Delta t, \dot{v}_n\Delta t^2, \ddot{d}_n\Delta t^2, \ddot{v}_n\Delta t^3 \right\}^T$$
$$\text{GA-234:}\quad \mathbf{X_n} = \left\{ d_n, v_n\Delta t, \dot{d}_n\Delta t, \dot{v}_n\Delta t^2, \ddot{d}_n\Delta t^3, \ddot{v}_n\Delta t^4 \right\}^T$$

and $\mathbf{A}$ is the corresponding amplification matrix. The coefficients of the amplification matrices depend on ω, ξ, Δt, and the coefficients α, β_i, and γ. The matrices can be easily derived using symbolic mathematical software but are omitted here for the sake of brevity. For more details, refer to [10]. The spectral radius, $\rho(\mathbf{A})$, is defined as

$$\rho = \max(|\lambda_1|, |\lambda_2|, \ldots, |\lambda_d|), \tag{25}$$

where λ_i is the i-th eigenvalue of $\mathbf{A}$ and $d = 4, 6, 8$ for GA-2, GA-23 and GA-234, respectively. A scheme is unconditionally stable if $\rho(\mathbf{A}) \leq 1$ for any $\Delta t \geq 0$.

Figs. 1 and 2 show, respectively, the spectral radii versus the time step size and the eigenvalues of the amplification matrices in the complex plane for different values of ρ_∞. The methods are confirmed to be unconditionally stable, since all eigenvalues lie within or on the unit circle. The spectral radius does not exceed the value of one for any time step size Δt. Moreover, Fig. 1 shows that GA-23 and GA-234 shift the onset of significant numerical damping to larger time steps, which results in less numerical damping in the low-frequency regime compared to GA-2. To evaluate numerical dissipation and dispersion, the algorithmic damping ratio and the relative period error are defined as follows

$$\bar{\xi} = -\frac{\ln|\lambda|}{\bar{\Omega}} \qquad \text{and} \qquad \frac{\bar{T}-T}{T}, \tag{26}$$

where

$$\bar{T} = \frac{2\pi}{\bar{\omega}}, \qquad \bar{\omega} = \frac{\bar{\Omega}}{\Delta t}, \qquad \bar{\Omega} = \arg(\lambda). \tag{27}$$

Figs. 3 and 4 display the algorithmic damping ratios and relative period errors over the time step size, respectively. Notably, GA-23 and GA-234 exhibit smaller approximation errors compared to GA-2. The scheme GA-234 is more accurate than GA-23.

5. Backward difference formulae

For $\rho_\infty = 0$, GA-23 and GA-234 can be cast in the format of backward difference formulae as shown in [10]. BDF-23 is a linear combination of BDF-2 and BDF-3, while BDF-234 combines BDF-2, BDF-3, and BDF-4. For linear problems with correct initial conditions, the BDF methods produce identical results to their GA counterparts for $\rho_\infty = 0$. However, they lack time adaptability and user-controlled high-frequency damping. Nevertheless, integrating them into existing code based on

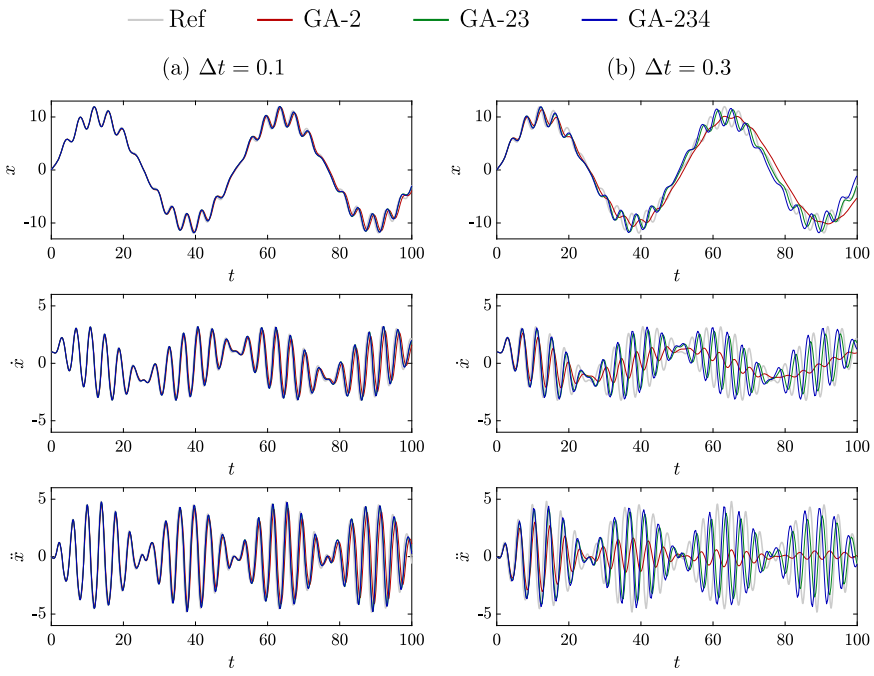

Fig. 19. Nonlinear two degree of freedom oscillator; solution obtained in x-direction with $\rho_\infty = 0$.

the standard backward difference formula is straightforward and immediately enhances accuracy at negligible additional storage cost. In the examples presented in Sections 7 to 11, BDF-23 and BDF-234 are represented by GA-23 and GA-234 with $\rho_\infty = 0$ (Boxes 9 and 10).

6. Comments on the comparison with the Bathe method

The Bathe method is a well-known composite scheme which combines the trapezoidal rule with the BDF-2 formula. Several variations of the Bathe method have been presented [2–4,28–30,32]. Any analysis or numerical results shown in the remainder of this work refer to the standard Bathe method with $\gamma = 2 - \sqrt{2}$ [3]. The approach taken in the development of the GA-23 and GA-234, based on the linear combination of second order and higher order schemes, is entirely different. The following remarks comment on computational cost and implementation, accuracy and suitability for modelling wave propagation of the two strategies.

Computational cost and implementation: Due to its multi-sub-step nature, the implementation of the Bathe method is more intrusive. It requires that two global systems are solved. In many cases the stiffness matrices involved are identical or differ only by scalar factors such that the matrix factorisation can be reused and the additional computational cost is small. For nonlinear problems, each sub-step requires the use of a Newton procedure and the computational cost per time step is generally more significant.

Accuracy: Fig. 5 shows the spectral radii for GA-2, GA-23, GA-234 and the Bathe method, while Fig. 6 shows the algorithmic damping ratio and the relative period error. Due to the larger computational cost, the Bathe method is considered with time step sizes of Δt and $2\Delta t$. These are distinguished by using the abbreviations B-Δt and B-$2\Delta t$, respectively. In the context of the comparison with GA-2, GA-23 and GA-234, the schemes B-Δt and B-$2\Delta t$, in a sense, represent upper and lower bounds of the performance of the Bathe method. In Figs. 5 and 6, it is observed that, for $\rho_\infty = 0$, GA-23 and B-$2\Delta t$ are of similar quality while GA-234 lies between B-$2\Delta t$ and B-Δt. Numerical results obtained with B-Δt and B-$2\Delta t$ are shown in Section 8.

Modelling wave propagation: The Bathe method has been demonstrated to be highly effective for solving wave propagation in elastic solid material [25,27]. Namely, discontinuities in the velocity are resolved relatively accurately. For GA-23 and GA-234, the combination of second order with higher order schemes results in improved accuracy but also introduces a requirement for more smoothness. Hence, the discontinuities associated with shock waves are dispersed faster than by the Bathe method, while smooth wave propagation is reproduced highly accurately by GA-23 and GA-234, as shown in Section 11.

$$\mathbf{M}\ddot{\mathbf{d}}_{n+1} + \mathbf{C}\dot{\mathbf{d}}_{n+1} + \mathbf{K}\mathbf{d}_{n+1} = \mathbf{F}_{n+1}$$
$$\ddot{\mathbf{d}}_{n+1} = \frac{10\,\dot{\mathbf{d}}_{n+1} - 15\,\dot{\mathbf{d}}_n + 6\,\dot{\mathbf{d}}_{n-1} - \dot{\mathbf{d}}_{n-2}}{6\,\Delta t}$$
$$\dot{\mathbf{d}}_{n+1} = \frac{10\,\mathbf{d}_{n+1} - 15\,\mathbf{d}_n + 6\,\mathbf{d}_{n-1} - \mathbf{d}_{n-2}}{6\,\Delta t}$$

Box 9. Summary of method BDF-23 for structural dynamics.

$$\mathbf{M}\ddot{\mathbf{d}}_{n+1} + \mathbf{C}\dot{\mathbf{d}}_{n+1} + \mathbf{K}\mathbf{d}_{n+1} = \mathbf{F}_{n+1}$$
$$\ddot{\mathbf{d}}_{n+1} = \frac{35\,\dot{\mathbf{d}}_{n+1} - 56\,\dot{\mathbf{d}}_n + 28\,\dot{\mathbf{d}}_{n-1} - 8\,\dot{\mathbf{d}}_{n-2} + \dot{\mathbf{d}}_{n-3}}{20\,\Delta t}$$
$$\dot{\mathbf{d}}_{n+1} = \frac{35\,\mathbf{d}_{n+1} - 56\,\mathbf{d}_n + 28\,\mathbf{d}_{n-1} - 8\,\mathbf{d}_{n-2} + \mathbf{d}_{n-3}}{20\,\Delta t}$$

Box 10. Summary of method BDF-234 for structural dynamics.

7. Example 1: linear single degree of freedom oscillator

To evaluate the performance and accuracy of GA-23 and GA-234, the single-degree-of-freedom system defined by Equation (23) is employed. The frequency is set to $\omega = 1$ resulting in an oscillation period of $T = 2\pi$. The initial displacement and velocity are specified as $d(0) = 1$ and $\dot{d}(0) = 0$.

Fig. 7 presents the responses obtained using the exact solution, the GA-2, GA-23, and GA-234 scheme. The responses are displayed for different time step sizes and values of ρ_∞. For larger time steps, GA-23 and GA-234 are substantially more accurate than GA-2, providing reduced numerical damping and smaller frequency errors. Notably, GA-234 is slightly more accurate than GA-23.

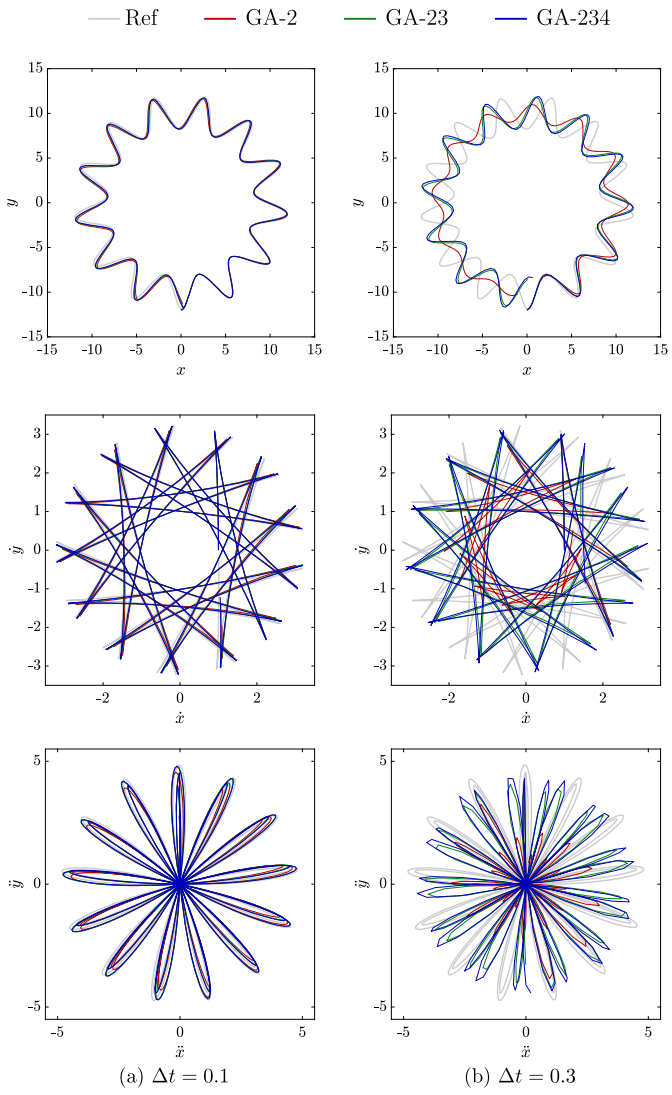

Fig. 20. Nonlinear two degree of freedom oscillator; phase space trajectories obtained with $\rho_\infty = 0$.

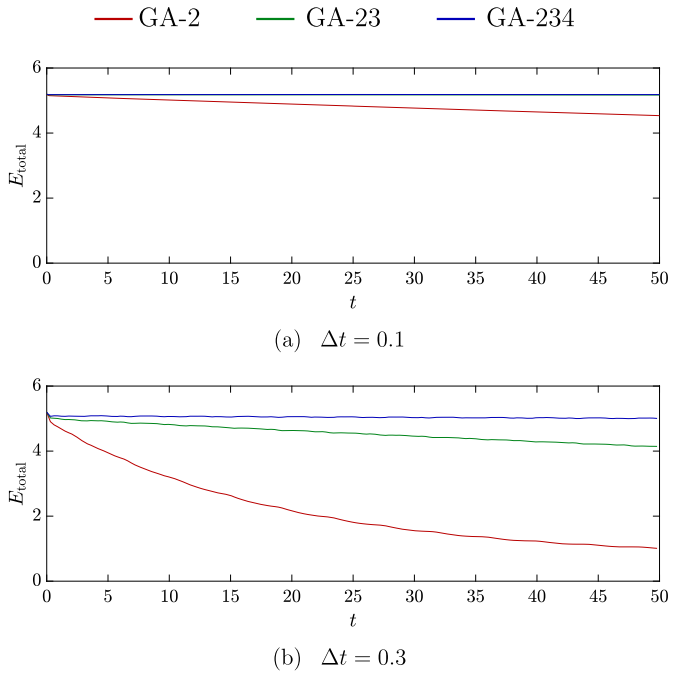

Fig. 21. Nonlinear two degree of freedom oscillator; evolution of the total energy over time obtained using $\rho_\infty = 0$.

Table 1
Linear stiff-soft spring system, free oscillation; comparison of frequencies and error.

Method	Frequency	Error (%)
Analytical	0.1125	-
GA-234 ($\rho_\infty = 0$)	0.1111	1.27
GA-23 ($\rho_\infty = 0$)	0.1108	1.54
GA-2 ($\rho_\infty = 0$)	0.1081	3.94
GA-234 ($\rho_\infty = 1/3$)	0.1113	1.13
GA-23 ($\rho_\infty = 1/3$)	0.1112	1.19
GA-2 ($\rho_\infty = 1/3$)	0.1104	1.91
B-Δt	0.1116	0.86
B-$2\Delta t$	0.1103	1.95

Fig. 8 displays the convergence of the numerical solutions for different values of ρ_∞. The error ϵ is determined by comparing the exact displacement $\tilde{d}$ with the numerical displacement $\bar{d}$ from each method, *i.e.*

$$\epsilon(t_N) = \sqrt{\frac{t_N}{N} \sum_{i=1}^{N} \left| \tilde{d}(t_i) - \bar{d}(t_i) \right|^2}, \tag{28}$$

where N is the number of time steps used in the respective computation to reach $t_N = 35$.

As ρ_∞ approaches 1, the differences between the methods decrease and eventually they all coincide with trapezoidal rule. For $\rho_\infty = 0$, the improvement in accuracy from GA-2 to GA-234 in the regime of time steps around $\Delta t = T/32$ is similar to that from the first order accurate method GM to the second order accurate scheme GA-2. This is also reflected in Fig. 7 where, for $\rho_\infty = 0$, GA-234 renders significantly more accurate results than GA-2. Hence, the new methods GA-23 and GA-234 offer substantial benefit in the range of time steps $T/50 < \Delta t < T/25$ which is highly relevant for industrial applications.

8. Example 2: linear stiff-soft spring system, free oscillation

A two-degree-of-freedom system is considered which consists of two equal point masses, $m_1 = m_2 = 1$. The masses are supported by two springs as shown in Fig. 9. The spring stiffnesses are $k_1 = 1$ and $k_2 = 10^7$. The time step size is set to $\Delta t = 0.5$. Due to the excessive stiffness ratio, the oscillation associated with the high frequency is not of interest and will not be resolved. The lower frequency results in an oscillation period of 8.897. The initial displacements are set to $\{0, 1\}$ while both initial velocities are zero. Fig. 10 shows the responses obtained from the different schemes considered in this work, including the Bathe method. The observed oscillation frequencies are summarised in Table 1.

As expected, the initial conditions cause spurious numerical oscillations for $\rho_\infty = 1$ (trapezoidal rule), which are effectively damped out if smaller values of ρ_∞ are used. In Fig. 10(a), for $\rho_\infty = 0$, the responses of GA-23, GA-234 and the Bathe method are far more accurate in terms of dissipation and frequency errors than GA-2. GA-23 is closely matched by B-$2\Delta t$, while the quality of the results obtained from GA-234 lies between those of B-Δt and B-$2\Delta t$. For larger $\rho_\infty > 0$, the accuracy of GA-2, GA23, and GA234 increases, with even GA-2 performing better than B-$2\Delta t$ for $\rho_\infty = 1/3$ in Fig. 10(b).

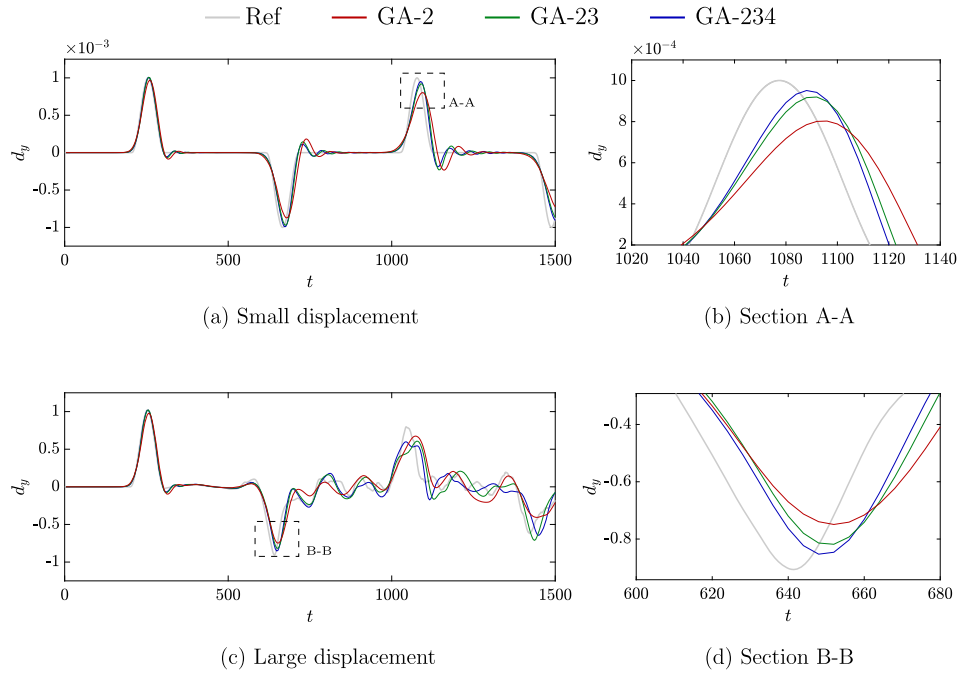

Fig. 22. Wave propagation on a string; vertical displacement at the midpoint obtained using $\rho_\infty = 0$ and $\Delta t = 4$ ms.

Table 2
Linear elastic cantilever beam; frequency comparison obtained with $\rho_\infty = 0$ and $\Delta t = 0.2$.

Method	Frequency	Error (%)
Reference	0.2453	-
GA-234	0.2448	0.21
GA-23	0.2431	0.90
GA-2	0.2397	2.29

9. Example 3: linear elastic cantilever beam

In this example, a linear elastic cantilever beam with length $L = 4$, height $H = 0.2$, Young's modulus $E = 15000$, Poisson's ratio $\nu = 0.35$ and density $\rho = 1$, is considered. The thickness in the third direction is $w = 1$. The beam is fully fixed on the left side and free at the other end. The employed mesh consists of 160 nine-noded plane stress elements, as shown in Fig. 11.

Initially, a point load $P = 0.2$ is applied at the central node of the free end. A steady-state analysis is then performed to obtain the static response, which is used as the initial condition for the dynamic analysis. Fig. 12 shows a typical deformed configuration. Fig. 13 displays the vertical displacement at the central node of the free end against time, obtained using GA-234 with $\rho_\infty = 0$ and $\Delta t = 0.1$. Figs. 14 and 15 respectively show the shear force and bending moment at the clamped end.

A mesh-dependent reference solution is computed using GA-234 with $\Delta t = 0.0005$ and $\rho_\infty = 0$ and yields a frequency of $f = 0.24531$, which deviates slightly from the lowest analytical frequency. Table 2 shows the frequency errors obtained with the different methods relative to the mesh dependent reference solution. The methods GA-23 and GA-234 clearly outperform the standard generalised-alpha method GA-2. Fig. 16 illustrates the frequency convergence for different values of ρ_∞.

10. Example 4: nonlinear two degree of freedom oscillator

This example assesses the performance of GA-2, GA-23, and GA-234 in a nonlinear setting by investigating the spring pendulum shown in Fig. 17. The pendulum has the initial length $l_0 = 10$, point mass $m = 1$, and spring stiffness $k = 25$. The initial conditions are set such that in the x-direction, the displacement is $x = 0$ and the velocity is $\dot{x} = 1$. In the y-direction, the displacement is $y = -12$ with velocity $\dot{y} = 0$.

The governing equations of the system can be written as

$$\ddot{x}\, m + N\,\frac{x}{l} = 0, \qquad \ddot{y}\, m + N\,\frac{y}{l} = 0, \tag{29}$$

where $N = \varepsilon k$ is the elastic normal force in the spring, and the strain is calculated as $\varepsilon = \ln(\lambda)$ with $\lambda = l/l_0$ and l being the current length. Fig. 18 displays the evolution of the elastic force over time, obtained using $\rho_\infty = 0$ and $\Delta t = 0.3$. Fig. 19 illustrates the evolution of displacement, velocity, and acceleration in the x-direction, while Fig. 20 shows phase space trajectories. Both figures depict the results for two time step sizes, $\Delta t = 0.1$ and $\Delta t = 0.3$, alongside a reference solution obtained using GA-234 with $\Delta t = 0.001$. Responses in the y-direction resemble those in Fig. 19 and have thus been omitted. The total energy of the system is given by

$$E_{\text{total}} = \frac{1}{2} m \left(\dot{x}^2 + \dot{y}^2\right) + k\left(\lambda \ln(\lambda) - \lambda + 1\right) l_0\,. \tag{30}$$

Fig. 21 shows the total energy for GA-2, GA-23, and GA-234, obtained using $\rho_\infty = 0$ and time step sizes $\Delta t = 0.1$ and $\Delta t = 0.3$. The figure shows that GA-23 and GA-234 conserve the total energy in the system far more accurately than GA-2.

11. Example 5: wave propagation on a string

A string of length $L = 20\,\text{m}$, cross-sectional area $A = 2.0 \times 10^{-4}\,\text{m}^2$, density $\rho = 1.14 \times 10^3\,\text{kg/m}^3$, and Young's modulus $E = 2.7$ GPa is considered. It is fixed at one end, while a constant horizontal force of 540 N and a prescribed vertical displacement are applied at the other end. The string is linear elastic, and the horizontal force causes a strain of 0.1%. The string is represented by 1000 two-noded linear elements using mass lumping. The resolution of the displacements is geometrically exact, and a global Newton-Raphson procedure is employed to obtain the solutions at each time step. The prescribed vertical displacement is

$$d(t) = \frac{D}{2} \times \left(1 - \cos\left(\frac{2\pi t}{100}\right)\right) \quad \text{for} \quad 0 < t < 100$$

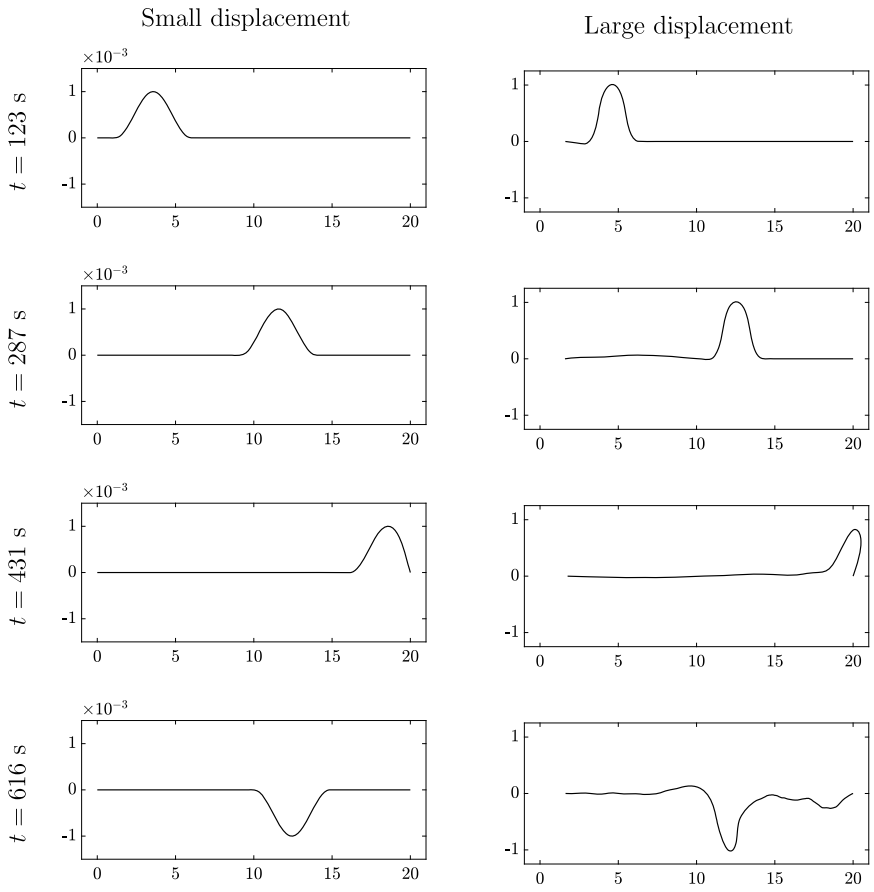

Fig. 23. Wave propagation on a string; snapshots of the wave travelling along the string.

and otherwise zero, where the time must be given in milliseconds. Two values of D are considered, namely, $D = 1$ mm and $D = 1$ m, which result in linear and nonlinear responses, respectively.

Fig. 22 shows the vertical displacement at the midpoint of the string, obtained using GA-2, GA-23, and GA-234 with $\rho_\infty = 0$ and $\Delta t = 4$ ms. A reference solution using GA-234 with a time step of $\Delta t = 0.01$ ms is also provided. The results of the simulations are consistent with previous findings, confirming that GA-23 and GA-234 outperform GA-2 in terms of numerical accuracy and reduced numerical dissipation. Fig. 23 captures snapshots of the string at different times. For the small displacement $D = 1$ mm, the wave propagates smoothly along the string, demonstrating typical wave motion. The large displacement, $D = 1$ m, causes chaotic nonlinear oscillatory behaviour after the wave reflection at the fixed end.

12. Conclusions

This paper presents the application of the GA-23 and GA-234 methods, originally proposed for first-order systems in [10], to the second order problem in structural dynamics. The newly formulated methods retain all characteristics of the original algorithms of [10]; they are implicit, unconditionally stable, second-order accurate, and effectively dampen undesired high frequencies. The performance of the new schemes is demonstrated in several numerical examples. All examples consistently demonstrate that GA-23 and GA-234 outperform the generalised-α method as they more effectively capture the desired frequencies and are noticeably more accurate. The differences between the proposed methods and the Bathe method are discussed. For $\rho_\infty = 0$, the methods GA-23 and GA-234 can be expressed as backward difference formulae, as shown in Section 5. The computer implementation of the proposed schemes is straightforward, and the computational cost does not exceed that of the standard generalised-α method.

CRediT authorship contribution statement

Eman Alhayki: Writing – original draft, Visualization, Formal analysis. **Wulf G. Dettmer:** Writing – review & editing, Supervision.

Declaration of competing interest

The authors declare that they have no known competing financial interests or personal relationships that could have appeared to influence the work reported in this paper.

Data availability

No data was used for the research described in the article.

References

[1] Arnold M, Brüls O. Convergence of the generalized-α scheme for constrained mechanical systems. Multibody Syst Dyn 2007;85:187–202.
[2] Bathe K-J. Conserving energy and momentum in nonlinear dynamics: a simple implicit time integration scheme. Comput Struct 2007;85:437–45.
[3] Bathe K-J, Baig M. On a composite implicit time integration procedure for nonlinear dynamics. Comput Struct 2005;83:2513–24.
[4] Bathe K-J, Noh G. Insight into an implicit time integration scheme for structural dynamics. Comput Struct 2012;98–99:1–6.
[5] Bazilevs Y, Calo V, Cottrell J, Hughes T, Reali A, Scovazzi G. Variational multiscale residual-based turbulence modeling for large eddy simulation of incompressible flows. Comput Methods Appl Mech Eng 2007;197(1):173–201.
[6] Behnoudfar P, Deng Q, Calo VM. High-order generalized-alpha method. Appl Eng Sci 2020;4:100021.
[7] Butcher J. Numerical methods for ordinary differential equations. Wiley; 2008.

[8] Chung J, Hulbert GM. A time integration algorithm for structural dynamics with improved numerical dissipation: the generalized-α method. J Appl Mech 1993;60(2):371–5.
[9] Dahlquist G. A special stability problem for linear multistep methods. BIT Numer Math 1963;3:27–43.
[10] Dettmer WG, Alhayki E. New implicit time integration schemes combining high frequency damping with high second order accuracy. J Comput Phys 2024;514:113260.
[11] Dettmer WG, Perić D. A new staggered scheme for fluid–structure interaction. Int J Numer Methods Eng 2013;93(1):1–22.
[12] Dettmer W, Perić D. An analysis of the time integration algorithms for the finite element solutions of incompressible Navier–Stokes equations based on a stabilised formulation. Comput Methods Appl Mech Eng 2003;192(9–10):1177–226.
[13] Dettmer W, Perić D. A computational framework for fluid–structure interaction: finite element formulation and applications. Comput Methods Appl Mech Eng 2006;195(41):5754–79. John H. Argyris Memorial Issue. Part II.
[14] He T. A strongly-coupled cell-based smoothed finite element solver for unsteady viscoelastic fluid–structure interaction. Comput Struct 2020;235:106264.
[15] Hilber HM, Hughes TJ. Collocation, dissipation and [overshoot] for time integration schemes in structural dynamics. Earthq Eng Struct Dyn 1978;6(1):99–117.
[16] Hilber HM, Hughes TJ, Taylor RL. Improved numerical dissipation for time integration algorithms in structural dynamics. Earthq Eng Struct Dyn 1977;5(3):283–92.
[17] Hughes TJR. The finite element method: linear static and dynamic finite element analysis. Englewood Cliffs, New Jersey: Prentice-Hall, Inc.; 1987.
[18] Jansen KE, Whiting CH, Hulbert GM. A generalized-α method for integrating the filtered Navier-Stokes equations with a stabilized finite element method. Comput Methods Appl Mech Eng 2000;190(3):305–19.
[19] Joosten MM, Dettmer WG, Perić D. On the temporal stability and accuracy of coupled problems with reference to fluid–structure interaction. Int J Numer Methods Fluids 2010;64(10–12):1363–78.
[20] Kadapa C, Dettmer WG, Perić D. Accurate iteration-free mixed-stabilised formulation for laminar incompressible Navier–Stokes: applications to fluid–structure interaction. J Fluids Struct 2020;97:103077.
[21] Kadapa C, Dettmer W, Perić D. On the advantages of using the first-order generalised-alpha scheme for structural dynamic problems. Comput Struct 2017;193:226–38.
[22] Kadapa C, Dettmer W, Perić D. A stabilised immersed framework on hierarchical b-spline grids for fluid-flexible structure interaction with solid–solid contact. Comput Methods Appl Mech Eng 2018;335:472–89.
[23] Kees C, Akkerman I, Farthing M, Bazilevs Y. A conservative level set method suitable for variable-order approximations and unstructured meshes. J Comput Phys 2011;230(12):4536–58.
[24] Kim H, Rundfeldt H, Lee I, Lee S. Tissue-growth-based synthetic tree generation and perfusion simulation. Biomech Model Mechanobiol 2023;22:1–18.
[25] Kim K-T, Bathe K-J. Accurate solution of wave propagation problems in elasticity. Comput Struct 2021;249:106502.
[26] Kim W, Choi SY. An improved implicit time integration algorithm: the generalized composite time integration algorithm. Comput Struct 2017;196:341–54.
[27] Kwon S-B, Bathe K-J, Noh G. An analysis of implicit time integration schemes for wave propagations. Comput Struct 2020;230:106188.
[28] Lee C, Bathe K-J, Noh G. Stability of the bathe implicit time integration methods in the presence of physical damping. Comput Struct 2024;295:107294.
[29] Malakiyeh MM, Shojaee S, Bathe K-J. The bathe time integration method revisited for prescribing desired numerical dissipation. Comput Struct 2019;212:289–98.
[30] Malakiyeh M, Shojaee S, Hamzehei-Javaran S, Bathe K-J. New insights into the β_1/β_2-bathe time integration scheme when l-stable. Comput Struct 2021;245:106433.
[31] Newmark NM. A method of computation for structural dynamics. J Eng Mech Div 1959;85(3):67–94.
[32] Noh G, Bathe K-J. The bathe time integration method with controllable spectral radius: the ρ_∞-bathe method. Comput Struct 2019;212:299–310.
[33] Pfaller M, Hörmann J, Weigl M, Nagler A, Chabiniok R, Bertoglio C, et al. The importance of the pericardium for cardiac biomechanics: from physiology to computational modeling. Biomech Model Mechanobiol 2019;18.
[34] Quarteroni A, Sacco R, Saleri F. Numerical mathematics, texts in applied mathematics. Springer Berlin Heidelberg; 2006.
[35] Sevilla R, Gil AJ, Weberstadt M. A high-order stabilised ale finite element formulation for the Euler equations on deformable domains. Comput Struct 2017;181:89–102.
[36] Wen W, Wei K, Lei H, Duan S, Fang D. A novel sub-step composite implicit time integration scheme for structural dynamics. Comput Struct 2017;182:176–86.
[37] Wilson EL. A computer program for the dynamic stress analysis of underground structures. SESM Report No. 68-1. Berkeley: Division of Structural Engineering and Structural Mechanics, University of California; 1968.
[38] Wood W, Bossak M, Zienkiewicz O. An alpha modification of Newmark's method. Int J Numer Methods Eng 1980;15(10):1562–6.